J. Electrochem. Sci. Eng. **13(2)** (2023) 421-436; http://dx.doi.org/10.5599/jese.1638

Open Access : : ISSN 1847-9286
https://pub.iapchem.org/ojs/index.php/JESE

Original scientific paper

Post-heat treatment of electrochemically carburized low-carbon steel

Chan On Sow[1], Wong Min Jin Karen[1], Saffuan Awg Bahrin[2], Bih Lii Chua[1], Gan Jet Hong Melvin[3,✉] and Nancy Julius Siambun[3,✉]

[1]*Faculty of Engineering, Universiti Malaysia Sabah, Jalan UMS, Kota Kinabalu 88400, Sabah, Malaysia*

[2]*Mechanical Engineering Department, Politeknik Kota Kinabalu, Jalan Politeknik, Kota Kinabalu Industrial Park, Kota Kinabalu 88460, Sabah, Malaysia*

[3]*Centre of Research in Energy and Advanced Materials, Faculty of Engineering, Universiti Malaysia Sabah, Jalan UMS, Kota Kinabalu 88400, Sabah, Malaysia*

Corresponding authors: ✉ melvin.gan@ums.edu.my; ✉ nancyjs@ums.edu.my

Received: December 14, 2022; Accepted: February 14, 2023; Published: February 19, 2023

Abstract

Limited studies are available on post-heat treatment (tempering/annealing) of electrochemically carburized low-carbon steel, which can relieve internal stresses induced by the quenching process. In this study, the electrochemical carburization was carried out using the electrolyte mixture of sodium carbonate (Na_2CO_3) and sodium chloride (NaCl) under a CO_2 gas environment and 800 °C. The samples were then quenched in either water or oil. The peak hardness of the water-quenched sample (WQ) was higher than the oil-quenched sample (OQ). Comparatively, post-heat treated (tempered and annealed) samples showed lower peak hardness compared to quenched samples. An optical microscope was used to observe microstructural changes, while X-ray diffraction (XRD) was used to examine metal phases within all samples. The full width at half maximum (FWHM) of the martensite peak supported the stress relief in both tempered and annealed samples. Scanning electron microscope (SEM) with energy dispersive X-ray (EDX) was applied to determine the elemental composition of as received and electrochemically carburized and quenched low-carbon steel samples. The carbon content of the WQ sample was relatively higher than the OQ sample, whereas the tempered samples showed higher carbon content compared to the annealed samples, but both were lower than for quenched samples. Electrochemical carburization increased the carbon content and improved the hardness, while the tempering or annealing process relieved internal stresses that resulted in the hardness reduction.

Keywords

Steel; electrochemical carburization; molten salt; quenching; tempering; annealing

Introduction

The hardness of steel is defined as the ability to withstand localised deformation or resist the change in shape [1,2]. Several studies claimed a linear correlation between yield strength and tensile strength with the hardness of steel [3]. Furthermore, the behaviour of wear is affected by high hardness, seen as less abrasion on the parts subjected to high friction stress, resulting in longer service life of the steels [4].

Low-carbon steels with less than 0.3 wt.% carbon content consisted mostly of ferrite. Ferrite, which is the softest phase of steel, makes low-carbon steel have high machinability but low hardness [5]. The hardness of low carbon steels has usually been increased by the carburization process in molten salt, which increases the carbon content at the surface. In the early stage of molten salt carburization, the conventional carburization used a cyanide bath ($Ba(CN)_2$) as the electrolyte under heating for a period of time. However, the production of toxic discharge from this process led to the utilization of other types of electrolytes. Thus, an alternative method, electrochemical carburization, known as molten salt electro-carburization, was introduced to replace conventional carburization [6]. The molten salt electrochemical carburization was implemented to increase the carbon content on the surface of low-carbon steel and improve its hardness, wear resistance, and contact fatigue [6]. Furthermore, the continuous carbon dioxide (CO_2) supply into the system during the electrochemical carburization process successfully improved the hardness of the carburized mild steel [7]. The internal strain, induced due to the carbon atoms interstitially present in the crystal lattice of iron after the electrochemical carburization, caused the increment in hardness [8]. Moreover, the improved hardness of electrochemically carburized mild steel showed the reduced severity of adhesive wear and the tendency of the worn surface to fracture, resulting in a longer lifespan of mild steel [9]. The rapid cooling process (known as the quenching process) also improves microhardness, related to the resistance to slip and dislocation, by altering the primary phases [10].

Heat treatments involve heating the steel to a certain temperature and eventually quenching it to room temperature in order to produce the desired microstructure of steel [11]. Various cooling rates of different quenching media (water, oil, *etc*.) will affect the hardness of steel, where a fast cooling rate provides better hardness performance [12]. The effect of quenching after the electro-chemical carburization process improves hardness due to the formation of martensite [13]. It was already found that a high level of residual stresses was induced after the quenching process due to the severe thermal gradient at the surface and core of the workpiece [14]. In addition, the presence of residual macro-stresses after cutting led to the distortion of the steel [15]. A high level of residual stress distorts the manufacturing process, which results in cracking and general instability of the steel. It was shown that residual stress leads to the cracking of metal in the corrosive environment. Moreover, a fast cooling process such as quenching will cause quench cracks [16]. Hence, an idea was triggered to apply the post-heat treatment of low-carbon steel after electrochemical carburization and quenching to relieve the quenched steel's internal and residual stresses and improve its properties. It was shown that mechanical properties such as toughness, hardness and ductility could be improved by the post-heat-treatment by relieving internal stresses [10]. The tempering process diminishes the brittleness and improves the strength of the metal, while the annealing process refines the grain structure, which makes metals more ductile and softer. The post-heat treatment of metal is almost similar to the post-weld heat treatment (PWHT), which was used to reduce the residual stress and achieve better performance of the weld [17]. The PWHT ensures dimensional stability and reduces residual stress along the heat-affected zone of weldment, which

improves welded joints' performance. This is similar to the residual stress relief performed through the post-heat treatment of quenched steel [18].

In this study, the low-carbon steel was electrochemically carburized using Na_2CO_3-NaCl electrolyte in the carbon dioxide environment. The effect of quenching medium, water or oil, was investigated for electrochemically carburized samples. Due to their preferable cooling rate, water and oil were selected to obtain the desired hardness of carburized samples. Post-heat treatment, tempering or annealing, was conducted after the quenching process to relieve the stress in the samples. Hardness, microstructure, structural determination, and elemental analysis of the electrochemically carburized low-carbon steel were performed to examine the effect of both quenching media and two different post-heat-treatment procedures (tempering and annealing).

To the best of our knowledge, there is a limited number of studies on the post-heat-treatment of electrochemically carburized low-carbon steel, which triggered the idea of this study. Measurements of the hardness of electrochemically carburized low carbon steel samples quenched in different quenching media and post-heat-treated (tempering/annealing) were carried out, together with microscopic images, metal phase analysis and elemental determination. The combination of heat treatment processes such as electrochemical carburization, quenching and post-heat treatment (tempering/annealing) are expected to provide an alternative method to improve the properties of low carbon steel aside from the conventional heat treatment.

Experimental

Electrochemical carburization (electro-carburization process)

Low carbon steel samples with dimensions of 2.5×2.5×2.5 cm (length×width×height) were utilized in this study. Each sample surface was further ground to remove contaminants and rust. After grinding, the sample was connected to the cathode prior to the electrochemical carburization process. The low-carbon steel sample acted as a cathode, while the stainless-steel rod was used as an anode. The distance between electrodes was about 2.3 cm. The electrolyte used was a mixture of sodium carbonate (Na_2CO_3, Bendosen, purity ≥ 99.0 %) and sodium chloride (NaCl, Bendosen, purity ≥ 99.0 %) with a molar ratio of 4:1 (Na_2CO_3: NaCl). A total of 650 g salt was mixed and transferred into a 750 ml stainless-steel crucible.

The schematic diagram of the setup for the electrochemical carburization process is shown in Figure 1. A chamber was fabricated using stainless steel with a gas inlet and outlet to ensure the continuous flow of carbon dioxide gas (CO_2) in the chamber during the electrochemical carburization process. The top of the chamber was covered using alumina wool to minimize heat loss during the process. The crucible containing the electrolyte was placed in the stainless-steel crucible holder, then the holder was inserted in the middle of the chamber. A lid connected to the cathode, anode, and thermocouple was used to close and tightly seal the chamber.

The electrochemical carburization was carried out under the constant temperature of 800 °C for 3 h in the continuous supply of CO_2 (200 mL min^{-1}) with the constant voltage of 4.0 V supplied by the DC power supply (Agilent E3633A).

The reactions involved during the electro-carburization are as follows, equations (1)-(4) [7,8,19].

$$CO_3^{2-} + Fe + 4e^- \leftrightarrow Fe\text{-}C + 3O^{2-} \quad (1)$$

$$O^{2-} + CO_2(g) \leftrightarrow CO_3^{2-} \quad (2)$$

$$2O^{2-} \leftrightarrow O_2(g) + 4e^- \quad (3)$$

$$CO_2(g) + Fe \leftrightarrow Fe\text{-}C + O_2(g) \quad (4)$$

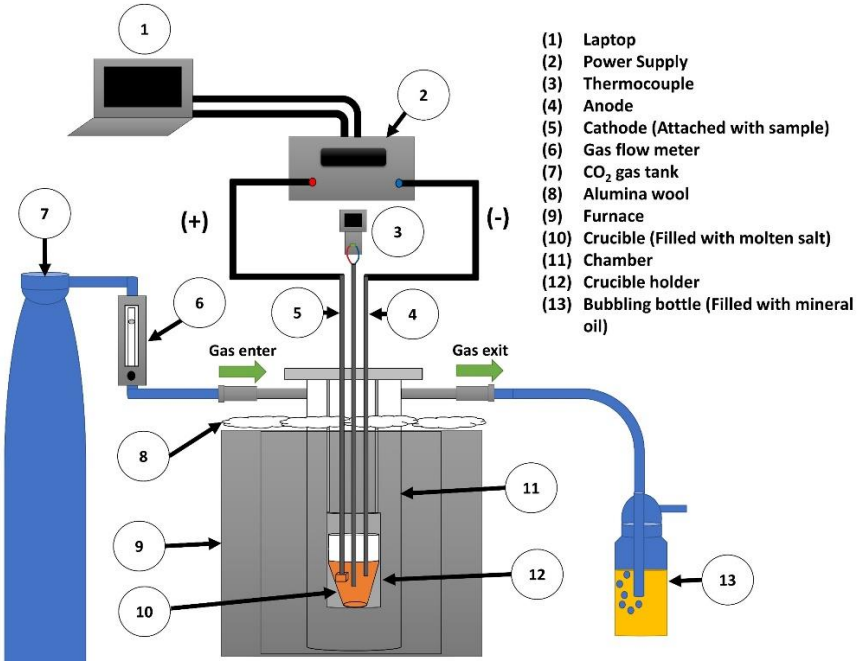

Figure 1. *Schematic diagram of the setup for electrochemical carburization process*

Based on the reaction (1), as the voltage was applied through the electrodes, the carbonate ions (CO_3^{2-}) in the electrolyte decomposed into carbon atoms and oxide ions (O^{2-}) at the cathode, where the sample is connected. The O^{2-} ions react with either CO_2 to form CO_3^{2-} (reaction (2)) or discharge at the anode as O_2 gas (reaction (3)). Reaction (4) shows the overall reaction during the electrochemical carburization process with the product of Fe-C, which is the carbon dissolved in the cathode sample [19].

After the electrochemical carburization, the samples were quenched in two types of quenching media: water and oil. The quenched samples were further tempered or annealed at 600 °C for 1 hour for the post-heat-treatment process. The tempered samples were cooled at ambient temperature, while the annealed samples were left to cool in the furnace.

As received and electrochemically carburized samples treated in different conditions were abbreviated as: as-received (AR), water quenched only (WQ), water quenched and tempered (WQ-T), water quenched and annealed (WQ-A), oil quenched only (OQ), oil quenched and tempered (OQ-T) and oil quenched and annealed (OQ-A), respectively.

Characterization of hardness, structure and composition of samples

The hardness from the outer surface towards the core of AR, WQ, WQ-T, WQ-A, OQ, OQ-T and OQ-A samples was measured using Vickers hardness tester (Mitutoyo AVK-C21) with the applied load of 10 N and 10 s of indentation time [8,13,19]. The hardness from the outer surface towards the core (1000 µm) was taken with an interval distance of 100 µm as shown in Figure 2.

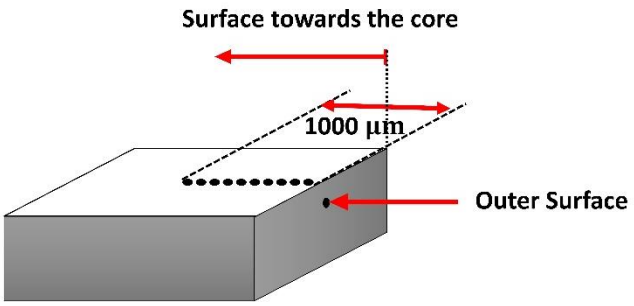

Figure 2. *Schematic illustration of the hardness test for as-received and electrochemically carburized samples*

Microstructure analysis was conducted using the optical microscope (20× and 50× magnification, Olympus BX60M). Prior analysis, the cross-section area and slightly polished outer surface of the sample was etched with nital solution (4 wt.% nitric acid in ethanol) for 30 s. X-ray diffraction (XRD, Rigaku Smartlab, λ = 0.15406 nm, Cu Kα radiation, 40 kV, 50 mA) was utilized to characterize the metal phase of samples in a continuous mode over a range of 2θ = 25 to 70° with a scan speed of 4.00° min^{-1} and step width of 0.01°. Elemental determination for the samples was examined using a scanning electron microscope (SEM, Hitachi S3400N) equipped with energy dispersive X-ray (EDX, QUANTEX Esprit 1.9) under magnification of 3000×, electron acceleration voltage of 15 kV and 10 mm working distance.

Results and discussion

Hardness and case hardening of as received and carburized samples

The electrochemically carburized samples underwent rapid cooling in two quenching media: water and oil. After the quenching process, the post-heat-treatment of tempering or annealing was carried out to relieve the residual stress of the electrochemically carburized samples. Figure 3 shows the average hardness measured from the outer surface (0 µm) to the depth of 1000 µm for the as-received (AR) and electrochemically carburized samples after quenching and post-heat treatment in different conditions.

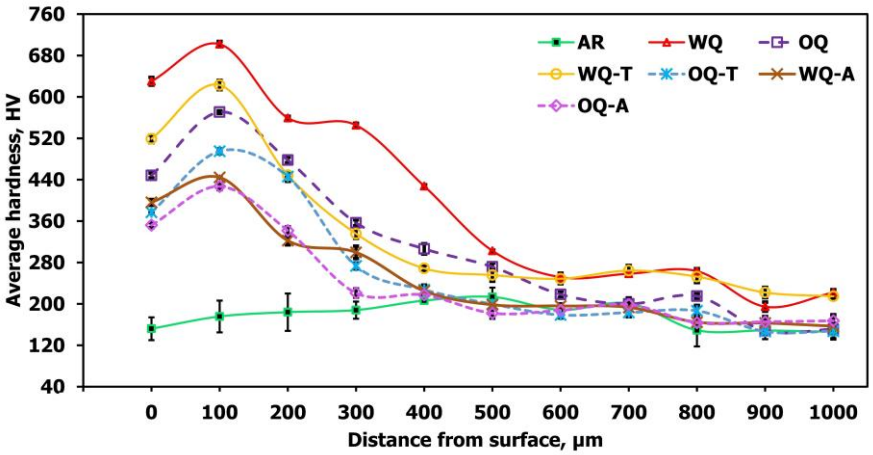

Figure 3. *Average hardness from the outer surface to the core of received and electrochemically carburized samples*

It is seen in Figure 3 that the outer surface (zero distance) hardness for all carburized samples was lower than the peak hardness detected at 100 µm depth. Hardness is gradually reduced from the peak and then levelled towards the 1000 µm depth. The point where the hardness started to level was estimated as the case depth. The case depth of water and oil-quenched samples (WQ and OQ) was in the range of 600 to 700 µm. Post-heat treated (tempered/annealed) samples exhibited similar case depth in the range of 450 to 550 µm. At 100 µm, the quenched samples exhibited relatively higher hardness than post-heat treated samples.

The average hardness of AR sample was 177±9 HV. WQ exhibited the highest peak hardness of 702±5 HV compared to other samples. Comparatively, the peak hardness of WQ is found to be lower than the values obtained for 3 hour electrochemical carburization process studied by Liew *et al*. [19] (795 HV with 660 µm case depth at 4.5 V) and Bahrin *et al*. [13] (1440 HV with 800 µm case depth at 4.0 V), with different experimental settings. The variation in peak hardness might be due to the distance between electrodes [13]. A smaller gap between the electrodes increases the transfer rate

of ions, which leads to higher carbon diffusion at the cathode. Moreover, the difference in the voltage applied during the electrochemical carburization process affected the hardness of the sample, too [8]. High voltage increased the charge and accelerated the reaction (1) in the molten salt bath, where the high activity of CO_3^{2-} caused the presence of more carbon at the cathode. In the study of Dewangan *et al.* [20], low-carbon steel was heated to 727 °C and then water quenched to room temperature. It was found that the Brinell hardness number (BHN) of the water-quenched sample was 357 BHN, within the range of 370 to 380 HV. Another heat treatment study on heating of AISI 1020 to 750 °C and water quenching resulted in the rise of the hardness of the sample from 191.7 HV (as received) to 254.3 HV [21]. A sample that underwent an electrochemical carburization process possessed higher surface hardness than the sample that was not electrochemically carburized, suggesting that electrochemical carburization produces high surface hardness. The higher hardness of electrochemically carburized samples has to be related to the carbon content formed at the cathode by equation (1).

Both ways of post-heat treatment of the WQ sample caused the reduction of peak hardness. Thus, the WQ-T sample showed a peak hardness of 623±9 HV, while WQ-A showed 444±1 HV. Both peak hardness values are lower compared to the WQ sample. The annealing process reduced the peak hardness more than the tempering process. The peak hardness of WQ-T was higher than WQ-A due to the cooling process during the tempering or annealing processes. In the tempering procedure, the sample was cooled at ambient temperature, whereas in annealing, the sample was left and cooled inside the furnace. Thus, the tempering procedure involved a faster cooling process, which caused insufficient time for carbon to react with oxygen in the atmosphere, and thus carbon became trapped within the sample, forming martensite. The annealing process involves a slower cooling process inside the furnace, where carbon might have sufficient time to react with oxygen [22]. The faster cooling process increased the hardness of the sample by delaying the formation of ferrite and promoting the formation of pearlite and martensite [23]. Typically, the range of high to low hardness is martensite > pearlite > ferrite [22].

The hardness of WQ-T and WQ-A samples was lower than WQ due to the stress relief and the structure rearrangement that lowers distortion occurring after martensite formation. For non-carburized samples, almost similar patterns can be observed with the exception that the overall hardness is comparatively lower than that of electrochemically carburized samples. For instance, according to Kanwal *et al.* [24], the initial hardness of low carbon steel in their study was 173.5 HV, while after heating at 960 °C and water quenching, the hardness was increased to 476.0 HV, and after the further tempering process at 550 °C, the hardness was reduced to 181.7 HV. The peak hardness of the OQ sample was 571 $\pm$ 3 HV. The peak hardness of oil-quenched samples was lower than water-quenched samples due to the difference in the cooling rate of the quenching medium. Similar results were reported by other studies, too [13]. At a slow cooling rate, the formation of pearlite is generated, which has been restricted for a high cooling rate. Therefore, most of the martensite has been formed through the high cooling rate of water quenching [25]. Martensite is formed with a highly distorted lattice structure, resulting in a high hardness of the sample [12]. Thus, the OQ sample, which experienced a slower cooling quenching process, consisted of pearlite and less amount of martensite, while the WQ sample consisted of a higher amount of martensite. Consequently, a lower peak hardness is shown for OQ compared to the WQ sample.

Similar to WQ samples, OQ samples also showed a reduction of peak hardness after tempering or annealing processes. The peak hardness of post-heat-treated samples decreased from 571 ± 3 HV to 495 ± 4 HV for OQ-T and to 367 ± 6 HV for OQ-A. The peak hardness of the WQ-T sample was higher

than the WQ-A sample due to the compressive stress. The compressive stress was due to the fast cooling in the tempering process, leading to higher peak hardness [22]. The increase of compressive stress increased the hardness of the sample, which will be further discussed below regarding FWHM results [23].

In general, the post-heat treatment process reduces the peak hardness of quenched samples, regardless of the quenching medium. Even though tempering or annealing lowered the hardness of the quenched sample, the hardness of both tempered and annealed samples was generally higher than the AR sample and provided better ductility (better machinability) compared to quenched samples. When the hardness was measured towards the core, it can be observed that the hardness decreased and eventually came close to the hardness of AR. In addition, the hardness decreased with the relaxation through the annealing process due to the reduction of dislocation density and strain hardening [26]. Similarly, the hardness also decreased due to the rearrangement of dislocations after stress-relieving tempering [27]. It is noticeable that all samples (except AR) showed lower surface hardness than the peak hardness at 100 μm depth. Further investigation *via* metallographic analysis and XRD was carried out. A discussion of the findings will be elaborated in the next section.

Structure and composition of as-received and electrochemically carburized samples

Figure 4 shows the optical microscopic images of the cross-section microstructure of AR and electrochemically carburized samples, indicating carbon penetration from the outer surface (right) towards the core (left). As visible in Figure 4(a), the AR sample is dominated by ferrite (white phase), while the presence of pearlite (dark phase) is visible on the grain boundaries only. Pearlite consists of lamellas of ferrite and cementite [28]. Nevertheless, the lamellar structure is not clearly visible in the image due to the relatively close orientation between ferrite and cementite. Another study also showed the presence of ferrite and pearlite in plain low-carbon steel [29]. Thus, the AR sample showed high ductility and low hardness due to the dominance of ferrite compared to pearlite [28].

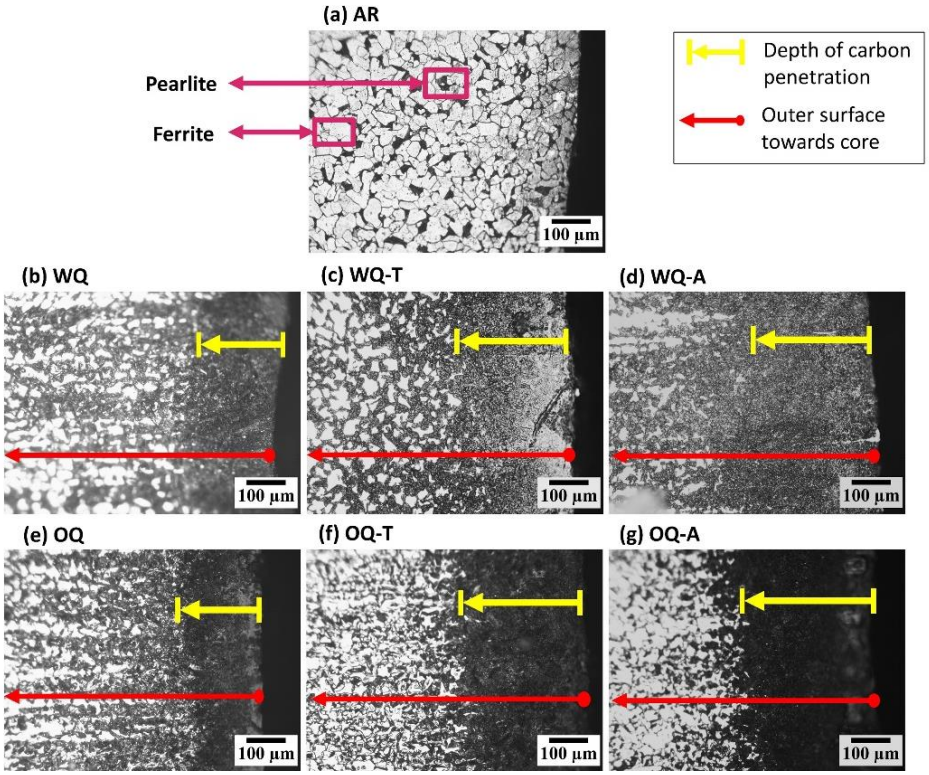

Figure 4. *Optical microscope images on the cross-section microstructure of (a) as-received and (b - g) electrochemically carburized samples*

The quenched electrochemically carburized samples (Figure 4(b) and (e)) and post-heat-treated samples (Figure 4(c-d) and (f-g)) showed a prominent dark microstructure compared to the AR sample, with the saturated dark region or dark layer near the surface. The dark microstructure consisted of phases containing high carbon content. As already reported by others, the dark microstructure layer consisted of martensite [13]. Martensite was formed when the carbon atoms became trapped within the octahedral interstitial sites of martensitic crystal structure [23]. Optical images at two different magnification levels (20× and 50×) for cross-section microstructure of AR, WQ and OQ samples are presented in Figure 5, showing the presence of martensite within the dark layer microstructure.

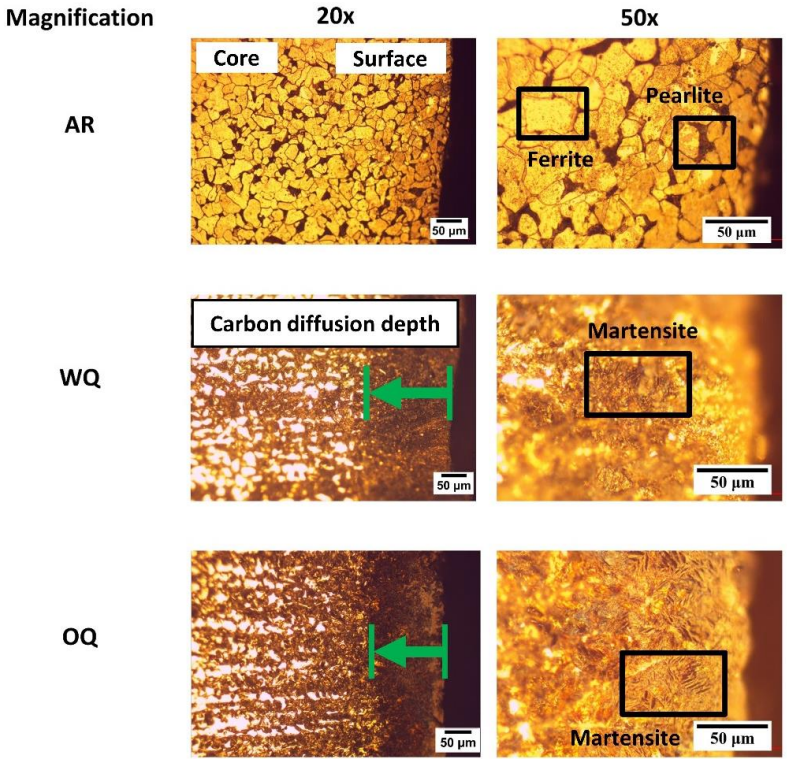

Figure 5. *Optical microscope images at different magnifications (20× and 50×) of cross-section microstructure for AR, WQ and OQ samples*

According to Figure 5, the microstructure of the AR sample consisted of a majority of ferrite (light phase) and pearlite (dark phase). For 20× magnification of WQ and OQ samples, there is a dark layer microstructure near the surface (right), not observed for the AR sample. The dark layer microstructure indicates the depth of the carbon diffusion layer from the surface to the core. From images with a 50× magnification level shown in Figure 5, the martensite present in needle-like or plate-like structures can be seen in both WQ and OQ samples. This indicates that due to the formation of martensite, the hardness for both WQ and OQ would be higher than for the AR sample.

The estimated dark layer distance from the surface to the core for WQ and OQ samples was between 230 to 245 μm, while for quenched and post-heat-treated samples (WQ-T, WQ-A, OQ-T and OQ-A), between 310 to 340 μm. In other words, tempering and annealing processes allow deeper distribution of carbon towards the core, seen as thicker dark layers for post-heat treated samples compared to quenched samples (Figure 4). In the re-heating process, the concentration difference of carbon was created between the inner part and outer part of the sample. This led to carbon diffusion, seen as dark microstructure diffusing to either the core region or to the surface, where it would cause decarburization [30]. On the other hand, the hardness of martensite depends

on the carbon content, and consequently, dispersion of carbon from the dark microstructure layer to the core would cause lower hardness of the post-heat-treated samples. Moreover, the peak hardness of all carburized samples in Figure 3 was within the dark layer distance. This is due to the presence of the martensite phase in the dark region, which improved the hardness of the samples compared to the rich ferrite phase in AR.

Based on the observation of microstructures from the surface towards the core, the dark microstructure (carbon-rich phase) is still visible, especially on grain boundaries of quenched and post-heat-treated samples. Moving further inwards to the core, the dark microstructure is gradually reduced, suggesting a gradual reduction of the concentration of carbon too. Reduction of carbon concentration would result in a decrease in hardness, which is in full agreement with hardness profiles shown in Figure 3. It is noticeable that the hardness of WQ-T, WQ-A, OQ-T and OQ-A samples have levelled to 177±19 HV (AR average hardness) after 550 μm depth. It is interesting that even after 700 μm depth, the hardness of WQ and WQ-T samples remained higher than 177±19 HV, suggesting that carbon was distributed deeper towards the core.

The outermost dark microstructure layer near the outer surface showed a grey layer for post-heat treated samples. This is due to the oxidation of steel at high temperatures during either the tempering or annealing process. The presence of oxygen during the cooling process of tempering and annealing caused the reaction between oxygen and highly oxidized element such as ferrite to form iron oxide [19]. This led to a lower surface hardness of post-heat-treated samples than the peak hardness (at 100 μm). In other words, for post-heat-treated samples (tempered or annealed), some extent of decarburization occurred. Based on Zorc *et al.* [30], the oxidation and decarburization of the steel take place simultaneously in the oxidizing atmosphere during the annealing process. At high temperatures, the difference in carbon concentration between the inner parts and the steel surface caused carbon diffusion from the inner part toward the surface. The carbon atoms then reacted with oxygen gas and formed carbon monoxide and carbon dioxide [30]. At temperatures higher than 570 °C, iron typically oxidizes to form iron oxide. Decarburization happened when equilibrium carbon potential is achieved between the chemical potential of carbon in the atmosphere and carbon on the surface of the annealed sample [30]. Campos *et al.* [31] found that decarburization of the steel occurred for quenched and tempered samples, for which the decarburized layer was observed and affected the microhardness of the sample. Therefore, the decarburization of samples might decrease the carbon content and lower the content of martensite on the surface, thus causing a reduction of surface hardness.

Further investigation was carried out to analyse the phases present inside the dark region. The surface of the AR and electrochemically carburized samples were polished using 1 μm size diamond paste to remove approximately 30 μm of the sample surface. Samples were etched using a nital solution to unveil the microstructure at 30 μm depth. The corresponding optical images are displayed in Figure 6.

The microstructure of the AR sample shown in Figure 6(a) consisted mostly of ferrite, which contributes to the metal softness but exhibits good strength and moderate ductility. The microstructure of WQ shown in Figure 6(b) is dominated by the plate-like structure of martensite, which demonstrates higher hardness but a brittle feature. The hardness of the martensite depends on the carbon content of the steel, as higher carbon content contributes to high hardness. When the water-quenched sample was tempered, the martensite was transformed into tempered martensite, as shown by the image of the WQ-T sample in Figure 6(c). Since the tempered martensite has a lower hardness than martensite [32], the hardness of the WQ-T sample was found to be lower than the WQ sample.

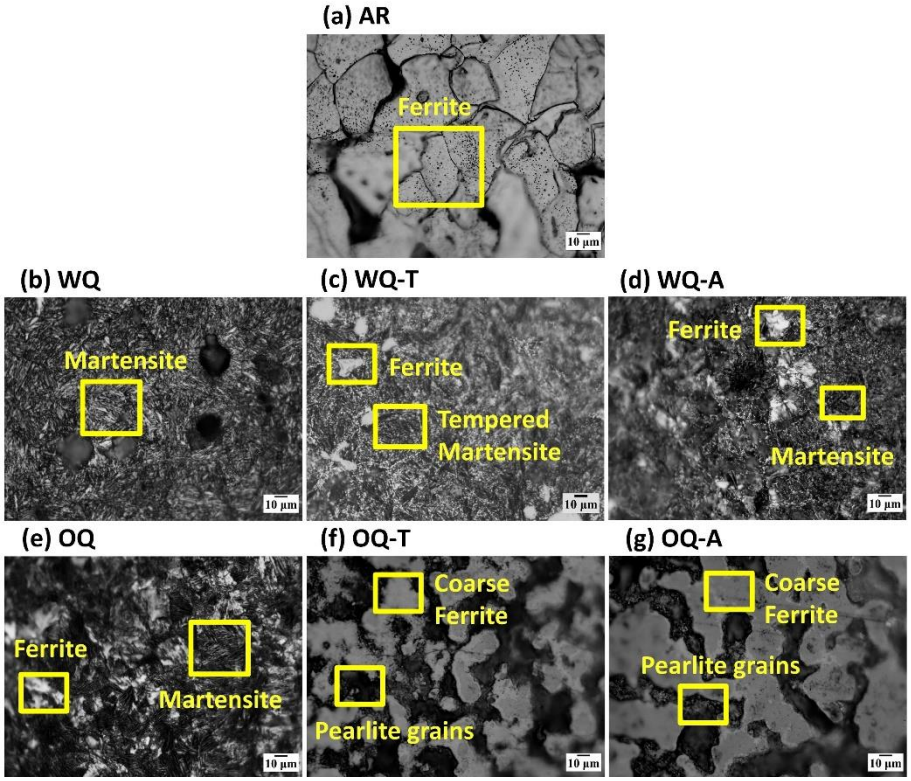

Figure 6. *Optical microscope images of slightly polished surface for (a) as received and (b - g) electrochemically carburized samples*

When the water-quenched sample was annealed, soft ferrite was present among the martensite phase [10], as shown in the microstructure of the WQ-A sample in Figure 6(d). The presence of the soft ferrite decreased the hardness of WQ-A compared to the WQ sample. As shown in Figure 6(e), the OQ sample consisted of a dispersion of fine ferrite within the martensite microstructure. The presence of fine ferrite caused lower hardness of OQ compared to the WQ sample. Tempering or annealing processes on OQ samples resulted in the formation of pearlite grains and coarse ferrite. Choi *et al.* [33] found that fine ferrite grains consisted of equiaxed and polygonal grain shapes that exhibited higher elastic modulus and hardness compared to coarse ferrite. This was due to the grain boundary that acted as a barrier of dislocation movement [33]. Hence, the presence of coarse ferrite in OQ-T and OQ-A samples contributed to the lower hardness compared to OQ samples.

The overall result is that the quenching process contributed to the high hardness due to the transformation into harder martensite. Formation of martensite, however, caused high distortion in the microstructure of the sample and therefore induced internal stresses, which led to low ductility and toughness of the sample. The tempering process was used to relieve the internal stress across the lath boundaries by allowing the local rearrangement of atoms [34]. Aside from tempering, annealing was also used to increase the ductility of the sample, soften the sample, relieve internal stresses and refine the structure to become homogeneous [35].

Further investigation using XRD (Figure 7) was carried out on the surface of AR and electrochemically carburized samples. In accordance with the image of AR in Figure 4(a), the XRD peaks of the AR sample showed the presence of only ferrite (JCPDS 06-0696) [36]. The XRD peaks for ferrite and martensite are located at 2θ = 44.7 and 44.6°, respectively, which are almost the same peak [36,37]. Based on Figure 6, the AR sample consisted mostly of ferrite, whereas WQ and OQ are dominated by martensite. The martensite peak (JCPDS 44-1292) [37] at 2θ = 44.6° (110) was visible for all electrochemically carburized samples (WQ, WQ-T, WQ-A, OQ, OQ-T and OQ-A), while

martensite peak at 2θ = 64.9° (200) was detected only for WQ and OQ, which are only quenched, and not post-heat treated samples.

It is noticeable that peaks of iron oxides, *i.e.,* magnetite, Fe_3O_4 (JCPDS 65-3107) [38] and hematite, Fe_2O_3 (JCPDS 33-0664) [39] were detected in all samples that underwent post-heat treatment. The presence of iron oxides (magnetite and hematite) in post-heat-treated samples supported the occurrence of decarburization and oxidation during the cooling process, where the samples were cooled in an oxidizing atmosphere, as discussed in the previous section.

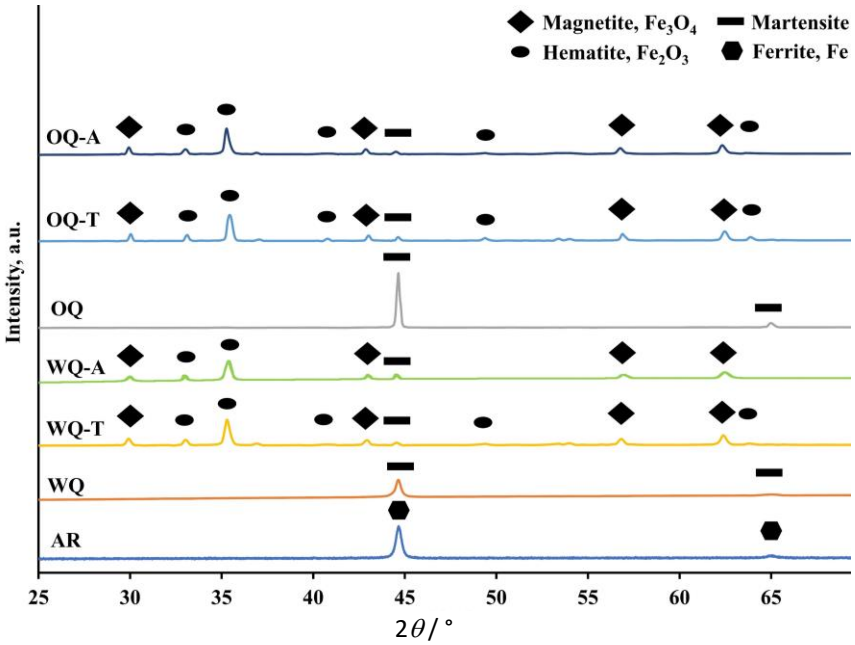

Figure 7. *X-ray diffraction (XRD) analysis for the outer surface of as received (AR) and electrochemically carburized samples (AR, WQ, WQ-T, WQ-A, OQ, OQ-T and OQ-A)*

The full width at half maximum (FWHM) at 2θ = 44.6° (martensite) for the electrochemically carburized samples is summarized in Figure 8. According to Fu *et al*. [15], the FWHM intensity of martensite is proportional to the hardness value. Thus, a higher FWHM value of martensite indicates a higher hardness value.

It is shown in Figure 8 that the WQ sample has the highest FWHM martensite intensity, followed by WQ-T, OQ, WQ-A (and OQ-T) and OQ-A samples. The FWHM martensite intensity is comparable to the hardness value of electrochemically carburized samples, as shown in the hardness profiles in Figure 3. It is interesting to mention that the stress relieved through the post-heat treatment was more prominent for WQ samples, where significant changes can be observed in Figure 8. For instance, the FWHM value for WQ-A and OQ-T samples was similar, but in Figure 3, WQ-A showed higher surface hardness than the OQ-T sample. This is due to the significant stress relieved from WQ to WQ-A sample, while the stress relieved from OQ to OQ-T sample was not so distinct. Nevertheless, the FWHM values functioning as hardness indicators support hardness profiles, as shown in Figure 3.

The hardness of electrochemically carburized quenched samples was reduced after the post-heat treatment. The FWHM value was found to be proportional to the residual stress [40], where high FWHM indicates the increment of the micro-strain along with the decrease of domain size of the metal, which could be relieved through the annealing process. In other words, the annealing process decreased the micro-strain while increasing the domain size (region inside the grains), reducing hardness [15].

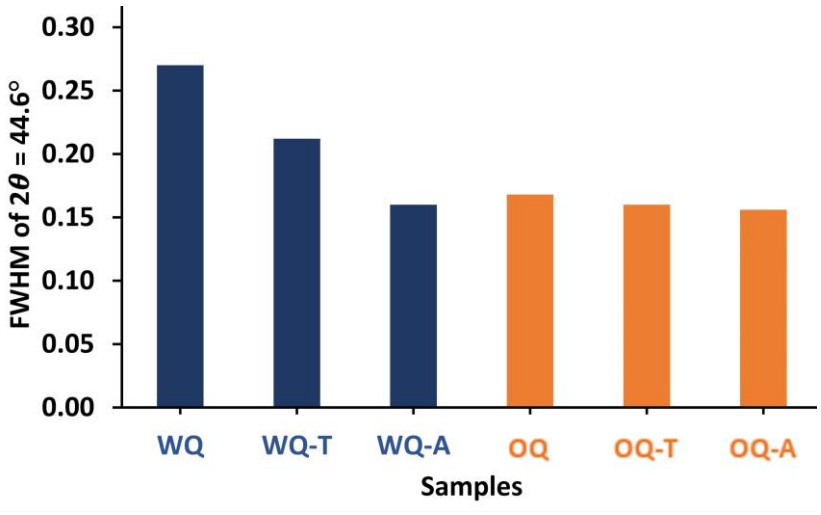

Figure 8. *Full-width half maximum (FWHM) for the electrochemically carburized samples at 2θ = 44.6° (martensite)*

Priyadarshini *et al*. [41] stated that the annealing process decreased the hardness of the sample due to the release of internal stresses. Zhang *et al*. [42] also found that FWHM is related to the grain distortion, residual stress, and dislocation density of the surface materials since higher FWHM showed higher hardening of the measured surface. The strain and surface defects were decreased after the tempering process [42]. In this work, tempering and annealing processes successfully relieved the stresses on the sample surface since lower FWHM was recorded for tempered or annealed samples (after either water or oil quenching).

SEM images with EDX mapping of oxygen and carbon were carried out on the outer surface of AR, WQ, WQ-T and WQ-A samples, as shown in Figure 9.

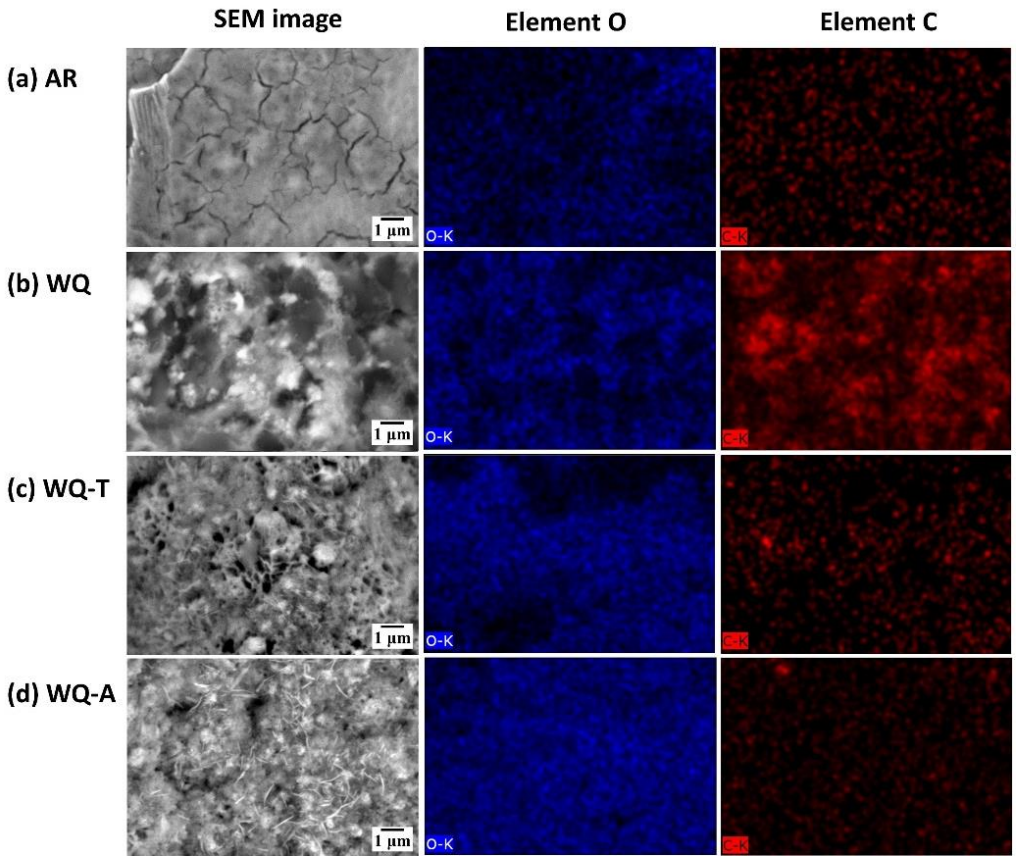

Figure 9*. SEM image with EDX mapping of (a) AR, (b) WQ, (c) WQ-T and (d) WQ-A samples*

The oxygen mapping of post-heat-treated samples is in agreement with XRD results. The oxygen mapping (blue colour) of tempered (Figure 9(c)) and annealed (Figure 9(d)) samples covered more area (concentrated) compared to WQ and AR samples. Moreover, the dark area (without oxygen) was more obvious for WQ and AR samples. It is also apparent that the WQ-A sample had higher oxygen concentration compared to WQ-T. The EDX analysis showed the carbon content on the outer surface of AR (2.79 wt.%), WQ (5.24 wt.%), WQ-T (5.16 wt.%), WQ-A (2.94 wt.%), OQ (4.73 wt.%), OQ-T (2.78 wt.%) and OQ-A (2.63 wt.%), respectively. Higher carbon content was in accordance with the higher surface hardness of samples. The EDX mapping also showed that, comparatively, WQ had higher carbon distribution (intense red colour). The red colour in WQ is more prominent compared to others, which indicates a high content of carbon that can be matched to the surface hardness depicted in Figure 3.

Conclusion

Different post-heat treatment procedures were applied to electrochemically carburized and quenched low-carbon steel samples in order to improve steel properties. Electrochemical carburization was performed in Na_2CO_3-NaCl molten salt at 800 °C in the presence of CO_2, and samples were quenched in either water or oil. Post-heat treatment was performed by either tempering involving faster or annealing involving a slower cooling process. Post-heat-treated samples generally showed lower peak hardness values than only quenched samples. Among post-heat-treated samples, annealed samples showed lower peak hardness than tempered samples. In difference to as received sample that showed only ferrite and quenched samples that showed only martensite phase, XRD of post-heat-treated samples showed a mixture of martensite, ferrite, and iron oxide (hematite and magnetite). The corresponding full width of half maximum (FWHM) values for the martensite XRD peak showed the relieving of stress after either tempering or annealing, which pointed again to the lower hardness of post-heat-treated samples. Optical images indicated a dark layer extending from the surface to the core of samples, that was found to be thicker for post-heat-treated than only quenched samples. This layer is ascribed to the carbon present as the martensite phase, distributed deeper within post-heat-treated than only quenched samples. The carbon content determined by EDX analysis was found to be lower, while the oxygen content was found to be higher for both post-heat-treated samples. These suggest simultaneous decarburization and iron oxidation processes that lower the hardness of post-heat-treated sample surfaces. The decrease in hardness could be related to relieving residual and internal stresses after the post-heat-treatment process.

References

[1] A. Di Gianfrancesco, *Technologies for chemical analyses, microstructural and inspection investigations* in: *Materials for Ultra-Supercritical and Advanced Ultra-Supercritical Power Plants,* A. Di Gianfrancesco, Ed., Woodhead Publishing, Sawston, Cambridge, 2017, 197-245. https://doi.org/10.1016/B978-0-08-100552-1.00008-7

[2] P. Smith, *Metallic Materials for Piping Components* in: *The Fundamentals of Piping Design*, P. Smith, Ed.,Gulf Publishing Company, Houston, Texas, 2007, 115-136. https://doi.org/10.1016/b978-1-933762-04-3.50012-6

[3] E. J. Pavlina, C. J. Van Tyne, Correlation of Yield strength and Tensile strength with hardness for steels, *Journal of Materials Engineering and Performance* **17** (2008) 888-893. https://doi.org/10.1007/s11665-008-9225-5

[4] G. S. O. Savabi, F. Nejatidanesh, M. H. Fathi, A. Navabi, Evaluation of hardness and wear resistance of interim restortive materials, *Dental Research Journal* **10(2)** (2013) 184-189. https://doi.org/10.4103/1735-3327.113338

[5] R. Evans, *Selection and testing of metalworking fluids* in: *Metalworking Fluids (MWFs) for Cutting and Grinding: Fundamentals and Recent Advances*, V. P. Astakhov, S. Joksch, Eds., Woodhead Publishing, Sawston, Cambridge, 2012, 23-78. https://doi.org/10.1533/9780857095305.23
[6] S. C. On, S. A. Bahrin, M. Gakim, W. Y. H. Liew, F. M. Tamiri, N. J. Siambun, A review on the development of electro-carburisation process, *IOP Conference Series: Materials Science and Engineering* **1217** (2022) 012010. https://doi.org/10.1088/1757-899x/1217/1/012010
[7] N. J. Siambun, D. A. Jewell, G. Z. Chen, Influence of CO_2 Gas in the Electro-Carburisation of Mild Steel, *International Journal of Chemical Engineering and Applications* **6(5)** (2015) 341-345. https://doi.org/10.7763/IJCEA.2015.V6.506
[8] N. J. Siambun, H. Mohamed, D. Hu, D. Jewell, Y. K. Beng, G. Z. Chen, Utilisation of Carbon Dioxide for Electro-Carburisation of Mild Steel in Molten Carbonate Salts, *Journal of The Electrochemical Society* **158(11)** (2011) H1117. https://doi.org/10.1149/2.017111jes
[9] L. Y. H. Willey, J. L. J. Ling, N. J. Siambun, Sliding wear behaviour of steel carburized using Na_2CO_3-NaCl, *MATEC Web of Conferences* **87** (2016) 02010. https://doi.org/10.1051/matecconf/20178702010
[10] S. N. Abdullah, N. Sazali, A. S. Jamaludin, Study on Thickness of Low Carbon Steel in Rapid Cooling Process, *Journal of Modern Manufacturing Systems and Technology* **4** (2020) 52-59. https://doi.org/10.15282/jmmst.v4i1.3546
[11] J. Grum, S. Božič, M. Zupančič, Influence of quenching process parameters on residual stresses in steel, *Journal of Materials Processing Technology* **114** (2001) 57-70. https://doi.org/10.1016/S0924-0136(01)00560-X
[12] M. A. Kowser, M. A. Motalleb, Effect of quenching medium on hardness of carburized low carbon steel for manufacturing of spindle used in spinning mill, *Procedia Engineering* **105** (2015) 814-820. https://doi.org/10.1016/j.proeng.2015.05.076
[13] S. A. Bahrin, W. L. Y. Liew, J. A. Janaun, S. K. A. Uvarajan, N. J. Siambun, The Influence of Quenching Medium on the Hardness and Microstructure of Electro-Carburised Low Carbon Steel, *The 1st Conference on Engineering, Technology and Education*, Politeknik Merlimau Melaka, Malaysia, 2016, 148-154.
[14] S. Masoudi, G. Amirian, E. Saeedi, M. Ahmadi, The Effect of Quench-Induced Residual Stresses on the Distortion of Machined Thin-Walled Parts, *Journal of Materials Engineering and Performance* **24** (2015) 3933-3941. https://doi.org/10.1007/s11665-015-1695-7
[15] P. Fu, R. Chu, Z. Xu, G. Ding, C. Jiang, Relation of hardness with FWHM and residual stress of GCr15 steel after shot peening, *Applied Surface Science* **431** (2018) 165-169. https://doi.org/10.1016/j.apsusc.2017.09.136
[16] V. D. Panchal, Relieving stress in stainless steels, *World Pumps* **2013** (2013) 28-32. https://doi.org/10.1016/S0262-1762(13)70030-0
[17] S. N. Abdullah, N. Sazali, A Mini Review on Low Carbon Steel in Rapid Cooling Process, *Journal of Advanced Research in Materials Science* **68(1)** (2020) 1-7. https://doi.org/10.37934/arms.68.1.17
[18] I. O. Oladele, D. B. Alonge, T. O. Betiku, E. O. Igbafen, B. O. Adewuyi, Performance Evaluation of the Effects of Post Weld Heat Treatment on the Microstructure, Mechanical and Corrosion Potentials of Low Carbon Steel, *Advanced Technologies and Materials* **44(1)** (2019) 41-47. https://doi.org/10.24867/atm-2019-1-007
[19] W. Y. H. Liew, R. Protasius, J. L. J. Ling, N. J. Siambun, N. A. Mohd-Lair, Reciprocating wear behavior of mild steel carburized using Na_2CO_3-NaCl, *Tribology International* **95** (2016) 406-418. https://doi.org/10.1016/j.triboint.2015.11.040

[20] S. Dewangan, N. Mainwal, M. Khandelwal, P. S. Jadhav, Performance analysis of heat treated AISI 1020 steel samples on the basis of various destructive mechanical testing and microstructural behaviour, *Australian Journal of Mechanical Engineering* **20** (2022) 74-87. https://doi.org/10.1080/14484846.2019.1664212
[21] I. F. MacHado, Technological advances in steels heat treatment, *Journal of Materials Processing Technology* **172** (2006) 169-173. https://doi.org/10.1016/j.jmatprotec.2005.09.007
[22] S. M. M. Rahman, K. E. Karim, M. H. S. Simanto, Effect of Heat Treatment on Low Carbon Steel: An Experimental Investigation, *Applied Mechanics and Materials* **860** (2016) 7-12. https://doi.org/10.4028/www.scientific.net/amm.860.7
[23] A. Çalik, Effect of cooling rate on hardness and microstructure of AISI 1020, AISI 1040 and AISI 1060 Steels, *International Journal of Physical Sciences* **4(9)** (2009) 514-518. https://academicjournals.org/article/article1380627919_Calik.pdf
[24] T. Kanwal, R. Nazir, S. Zulqernain, A. Salam, & Javaid Ahmad, Quench Hardening and Tempering Behaviour of A Low Carbon Steel, *Journal of Pakistan Institute of Chemical Engineers* **37** (2009) 51-53. https://lahore.comsats.edu.pk/Papers/Abstracts/380-8589025456608057058.pdf
[25] A. Rafaaltaweel, M. Tolouei-Rad, Effect of Quenching Media, Specimen Size and Shape on the Hardenability of Aisi 4140 Steel, *Emirates Journal for Engineering Research* **19(2)** (2014) 33-39
[26] F. Nazari, M. Honarpisheh, H. Zhao, Effect of stress relief annealing on microstructure, mechanical properties, and residual stress of a copper sheet in the constrained groove pressing process, *International Journal of Advanced Manufacturing Technology* **102** (2019) 4361-4370. https://doi.org/10.1007/s00170-019-03511-w
[27] V. Llaneza, F. J. Belzunce, Study of the effects produced by shot peening on the surface of quenched and tempered steels: Roughness, residual stresses and work hardening, *Applied Surface Science* **356** (2015) 475-485. https://doi.org/10.1016/j.apsusc.2015.08.110
[28] S. Dewangan, V. Vinod, K. Harshal, P. Manak, S. Ravikumar, M. Kr. Chowrasia, A discussion on mechanical behaviour of Heat-Treated low carbon steel. *Materials Today: Proceedings* **63** (2022) 362-367. https://doi.org/10.1016/j.matpr.2022.03.203
[29] D. H. Shin, B. C. Kim, Y. S. Kim, K. T. Park, Microstructural evolution in a commercial low carbon steel by equal channel angular pressing, *Acta Materialia* **48** (2000) 2247-2255. https://doi.org/10.1016/S1359-6454(00)00028-8
[30] M. Zorc, A. Nagode, M. Bizjak, B. Zorc, Decarburization of the Carbon Steel C45 During Annealing in Air, *Materials and Geoenvironment* **65** (2018) 167-178. https://doi.org/10.2478/rmzmag-2019-0005
[31] M. Campos, S. Kremel, T. M. Puscas, Y. Yu, D. Sánchez, J. M. Torralba, Effect of heat treatments on Cr-Mo steels based on astraloy CrM powder grade with manganese additions, *Materials Science Forum* **416-418** (2003) 82-88. https://doi.org/10.4028/www.scientific.net/msf.416-418.82
[32] N. M. Ismail, N. A. A. Khatif, M. A. K. A. Kecik, M. A. H. Shaharudin, The effect of heat treatment on the hardness and impact properties of medium carbon steel, *IOP Conference Series: Materials Science and Engineering* **114** (2016) 012108. https://doi.org/10.1088/1757-899X/114/1/012108
[33] Y. Choi, W. Yong Choo, D. Kwon, Analysis of mechanical property distribution in multiphase ultra-fine-grained steels by nanoindentation, *Scripta Materialia* **45** (2001) 1401-1406. https://doi.org/10.1016/S1359-6462(01)01176-9
[34] P. K. Jena, B. Mishra, M. RameshBabu, A. Babu, A. K. Singh, K. SivaKumar, T. B. Bhat, Effect of heat treatment on mechanical and ballistic properties of a high strength armour steel, *International Journal of Impact Engineering* **37** (2010) 242-249. https://doi.org/10.1016/j.ijimpeng.2009.09.003

[35] S. Ayyildiz, E. H. Soylu, S. Ide, S. Kiliç, C. Sipahi, B. Pişkin, H. S. Gökçe, Annealing of Co-Cr dental alloy: Effects on nanostructure and Rockwell hardness, *Journal of Advanced Prosthodontics* **5** (2013) 471-478. https://doi.org/10.4047/jap.2013.5.4.471

[36] T. Aljohani, M. Geesi, A. Kaiba, F. Khoshnaw, *The impact of gamma radiation on the corrosion properties of carbon steel and stainless steel*, European Corrosion Congress (EUROCORR 2019), Seville, Spain, 2019, 1-15.

[37] Y. Yang, M. F. Yan, Y. X. Zhang, Tribological behavior of diamond-like carbon in-situ formed on Fe 3 C-containing carburized layer by plasma carburizing, *Applied Surface Science* **479** (2019) 482-488. https://doi.org/10.1016/j.apsusc.2019.01.290

[38] Yusmaniar, W. A. Adi, Y. Taryana, R. Muzaki, Synthesis and Characterization of Composite UPR/Fe_3O_4 for Its Use as Electromagnetic Wave Absorber, *IOP Conference Series: Materials Science and Engineering* **196** (2017) 4-8. https://doi.org/10.1088/1757-899X/196/1/012033

[39] D. E. Fouad, C. Zhang, H. El-Didamony, L. Yingnan, T. D. Mekuria, A. H. Shah, Improved size, morphology and crystallinity of hematite (α-Fe_2O_3) nanoparticles synthesized via the precipitation route using ferric sulfate precursor, *Results in Physics* **12** (2019) 1253-1261. https://doi.org/10.1016/j.rinp.2019.01.005

[40] M. Vashista, S. Paul, Correlation between full width at half maximum (FWHM) of XRD peak with residual stress on ground surfaces, *Philosophical Magazine* **92** (2012) 4194-4204. https://doi.org/10.1080/14786435.2012.704429

[41] S. Priyadarshini, T. Sharma, G. Arora, Effect of Post Carburizing Treatment on Hardness of Low Carbon Steel, *International Journal of Advanced Mechanical Engineering* **4** (2014) 763-766. https://www.ripublication.com/ijame-spl/ijamev4n7spl_07.pdf

[42] M. Zhang, C. Chen, L. Qin, K. Yan, G. Cheng, H. Jing, T. Zou, Laser additive manufacturing of M2 high-speed steel, *Materials Science and Technology* **34** (2018) 69-78. https://doi.org/10.1080/02670836.2017.1355584